Assembly-oriented reliability analysis method for the top-connection structure of a nuclear fuel assembly

Yingdong Liu[a,b], Wenqiang Li[a,b,*], Jiahao Chen[a,b], Sitong Ling[a,b], Changfu Wan[a,b]

[a] School of Mechanical Engineering, Sichuan University, Chengdu 610065, China

[b] Innovation Method and Creative Design Key Laboratory of Sichuan Province, Chengdu 610065, China

Abstract: The nuclear fuel assembly is the core component of a nuclear reactor. In a pressurized water reactor fuel assembly, the top-connection structure connects the top nozzle to the guide thimble. Its performance reliability is essential for the stability of the nuclear fuel assembly. In this study, an assembly-oriented reliability analysis method for top-connection structures is presented by establishing an assembly-oriented top-connection structure parameter modeling method and a nonlinear contact gap and penetration correction method. A reliability model of the top-connection assembly structure, including multiple stochastic design variables, was constructed, and the overall reliability of the top-connection assembly structure was obtained via a Kriging model and Monte Carlo simulation. The acquired experimental data were consistent with real-world failure conditions, which verified the practicability and feasibility of the reliability analysis method proposed in this study.

Keywords: Assembly, Top-Connection Structure, Parametric Model, Approximation Model, Structural Reliability

1. Introduction

Nuclear energy is an important clean energy source [1-3]. The nuclear fuel assembly, as the core system in nuclear reactors, governs the safety and reliability of an

* Corresponding author. E-mail address: liwenqiang@scu.edu.cn.

entire nuclear energy system [4-6]. The top-connection structure is an assembly composed of multiple nuclear fuel assembly parts that serve as the connection between the top nozzle and the guide thimble in the pressurized water reactor (PWR) nuclear fuel assembly. During the lifting and transportation of a fuel assembly, the top-connection structure undergoes an acceleration that is a factor of 4 greater than the gravitational acceleration [7]. In the case of systematic structural failure, the entire nuclear fuel assembly faces significant potential safety hazards.

To date, reliability analysis of the top-connection structure of nuclear fuel assemblies relies heavily on physical experiments, which can be both expensive and time-consuming. Numerical simulations have gained popularity in recent years [8-10]. However, compared to the numerical simulation reliability analysis of an individual part, the analysis of the top-connection structure is a typical reliability analysis of an assembly structure that contains several related and mating assembly components. The marginal analysis error of any component has a considerable impact on the overall assembly reliability. In addition, owing to the existence of different assembly surface mating types in the assembly, the gap and penetration relationship of each contact surface in the assembly significantly affects the accuracy of the assembly reliability analysis. Therefore, developing a reliable analysis method for assemblies remains a challenging international focus.

In recent years, numerous studies have been conducted using numerical simulations of the top-connection structure of nuclear fuel assemblies and their associated structures [11,12]. Wang et al. [13] established a numerical simulation model for a top-connection structure using finite element analysis and investigated the tensile process of the top-connection structure. Liu [14] analyzed the strength of the top nozzle during transportation and lifting by simplifying the top-connection structure into a fixed connection. Yoo et al. [15] established a finite element model of a spacer grid that simulated its static and dynamic mechanical properties and compared it with physical experiments to verify the accuracy of the model, laying a good foundation for subsequent spacer grid optimization. Duan and Zhao [16] utilized CFX software to build a geometric model of a bottom nozzle and performed numerical simulations of

the bottom nozzle at different flow rates and split ratios. Wu et al. [17] conducted a mesh sensitivity analysis on the top nozzle, upper core plate, and top grid in the top fuel section of a reactor using computational fluid dynamics (CFD and compared the calculated pressure distribution with the corresponding experimental results. Su et al. [18] investigated the stress and bearing capacity of a CF3 fuel assembly bottom nozzle using a finite element analysis and load tests. Their results showed that the stress under each condition was in accordance with the American Society of Mechanical Engineers (ASME) code and that the bearing capacity satisfied the design requirements of the CF3 fuel assembly. Wei et al. [19] conducted a numerical study on the coolant flow in the top nozzle of a fuel assembly based on CFD and developed a numerical simulation method for the top-nozzle drag characteristics. The resistance characteristics were analyzed and evaluated to determine the resistance coefficient of the top nozzle. Dyk and Zeman [20] proposed a vibration modeling method for guiding the thimble in nuclear fuel assemblies and analyzed the effect of the maximum dynamic lateral deformation of the guide thimble on the radial gap of the spacer grid. Xu et al. [21] developed a CFD model for transverse flow in the top section of the AP1000 core, including the top-connection structure, and obtained a reasonable transverse flow velocity in the top section of the AP1000 core. Zhao et al. [22] established a nonlinear finite element model of a fuel assembly and conducted lateral stiffness, forced vibration, and impact experiments to verify its accuracy.

Despite the aforementioned studies probing the characteristics of top connections and associated structures, two major issues remain unaddressed. First, most of the studies were simulations of the top-connection structure and associated individual parts, while the system reliability analysis of the top-connection structure as an assembly was not included. Second, the design parameters in the numerical simulation analysis of the top-connection structure were commonly set to constant values. However, under real-world working conditions, multiple design parameters, including material properties and physical dimensions, have exhibited certain random errors. Hence, the key solution is to improve the reliability of the analysis in the presence of random multidesign parameter errors. In light of this, in the current study, we propose an assembly-oriented

top-connection structure reliability analysis method and process with an assembly-oriented parametric modeling and correction method for each contact surface in the assembly and an assembly-oriented reliability analysis method for the top-connection structure. An assembly-oriented approximation model for the reliability of the top-connection structure is also established. A Monte Carlo simulation (MCS) was deployed to perform a reliability analysis of the top-connection structure with multidesign parameter randomness, enabling the failure probability and reliability of the top-connection structures to be obtained. The proposed method demonstrates sound conformity with the physical experimental data and can be widely adopted in the reliability analysis of complex structures with assembly relations.

2. Assembly modeling and contact surface correction methods

Unlike the individual parts, an assembly structure is composed of multiple parts. Reliability analysis of the assembly system is highly nonlinear because the parts are intercoupled, making it difficult to guarantee calculation accuracy. There are three crucial elements in safeguarding the accuracy of the reliability analysis of assembly structures: determining the parametric modeling of the assembly structure, establishing the correlations between each assembly unit, and determining the connection and penetration relations between each assembly unit. In this study, a parametric modeling method for assemblies and a correction method for the contact gap and penetration of the contact surfaces between each assembly part were established, thereby providing an effective solution to fluctuations in the accuracy of the assembly reliability analysis.

2.1 Parametric modeling method for assembly systems

Assembly parameters are interrelated and mutually restricted. Consequently, the correlation between each parameter should be considered to establish the mapping relations between every design parameter, as well as the mapping relations between design parameters and mating-surface parameters, to ensure that the mating relations between the parts remain valid when the assembly model is updated. Mating between the parts of the assembly is achieved by matching the features of the parts, and a contact surface can be considered as a match of multiple features between two parts. To avoid

conflicting design variables caused by part modeling when updating the assembly, a parametric modeling method for assembly oriented systems was devised.

First, the design variables of each part were determined, and the corresponding features of each design variable were determined accordingly. Subsequently, the decoupling relations between the design features and design variables were completed by transforming the design-associated matrix to achieve mutual independence of the design variables. Therefore, if a certain design variable is changed, it does not cause conflicts with other design variables. Finally, the assembly was transformed based on features from the contact relations between parts to the contact relations between design variables. In this manner, the mating between parts of the assembly can be controlled using design variables, as shown in Figure 1.

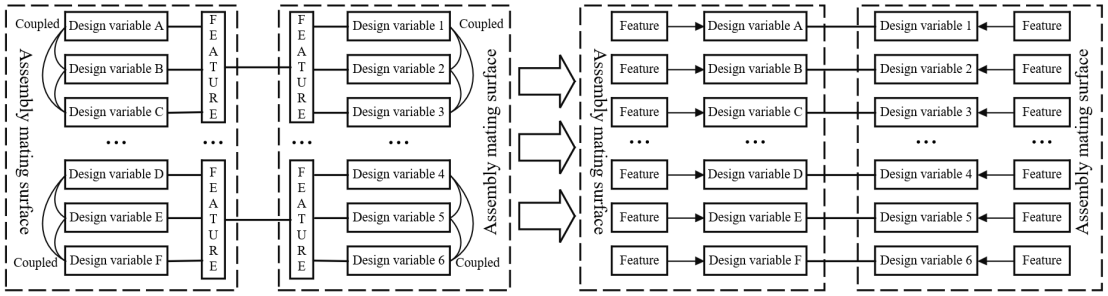

Figure 1. Parametric modeling method for assembly-oriented systems

The nuclear fuel assembly top-connection structure, as a typical assembly model, contains three contact faces: the contact between the top nozzle and connection-sleeve outer surface, the contact between the connection-sleeve inner surface and the locking-thimble outer surface, and the contact between the guide-thimble and connection-sleeve inner surfaces. Parameterization was performed for these contact faces and the design variables of each part were determined, as shown in Figure 2.

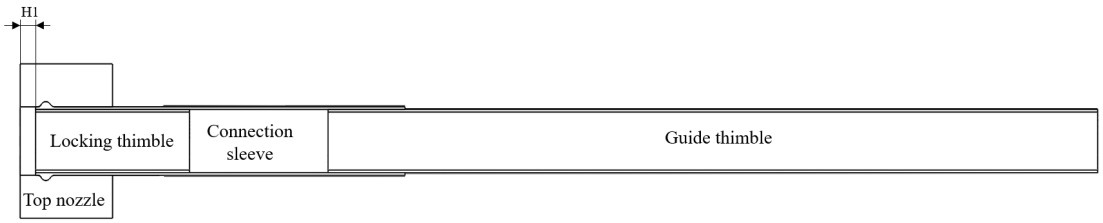

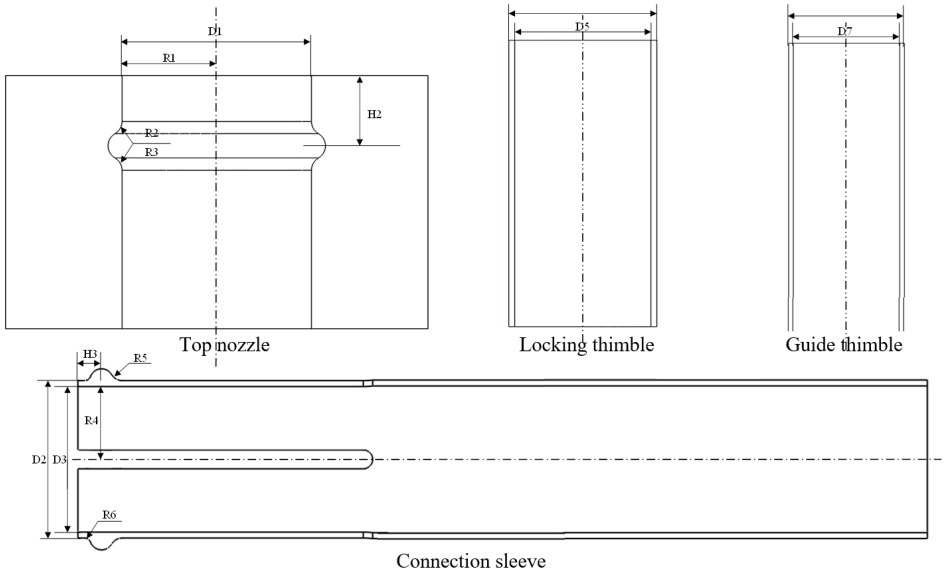

Figure 2. Schematics of the top-connection structure design parameters

Each part of the top-connection structure contained one parameter, and the design variables were independent of each other. Therefore, the mating surfaces of the top-connection structure correspond to the design parameters of each part, specifically D1–D2, R2–R6, R3–R5, D3–D4, and D6–D3. The links and equation constraints among the design parameters were established, as listed in Table 1, to ensure that the mating relationships between the parts remained valid when the top-connection structure model was updated.

Table 1. Mapping relations between the design parameters

R1=D1/2	R2=R3	D2=D1	R5=R3
H1+H3=H2	D4=D3	D6=D3	R4=D3/2
	D3<D2	D5<D4	D7<D6

Seven part design parameters were obtained by mapping the relations: D1, H2, R2, D5, D3, R6, and D7. The remaining eight parameters were obtained from the seven parameters by mapping relationships.

2.2 Contact surface gap and penetration value correction method for assembly systems

Errors occur between the mating surfaces during the assembly process; these have direct effects on the gap and penetration values between the contact surfaces. In addition, the quality of the modeling mesh affects the contact surface gap and penetration values

of an assembly. In this study, a correction method for the initial penetration and gap of the contact surfaces was developed. This may be utilized in the following circumstances: When there is an initial gap between the contact surfaces of the assembly, the gap can be supplemented to facilitate surface contact or, in the case of slight penetration between the two contact surfaces, the common penetration area can be removed by adjusting the contact surfaces. The adjustment method is shown in Figure 3, in which the penetration area is marked in red.

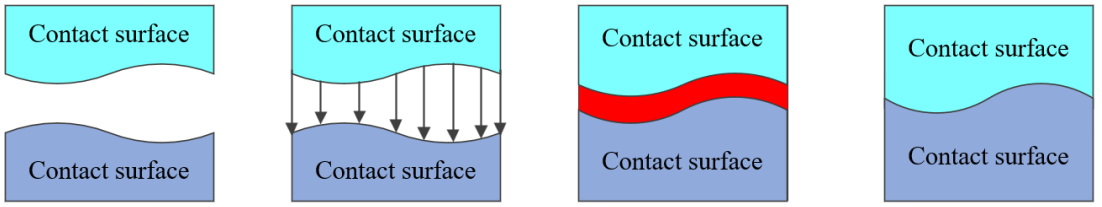

Figure 3. Contact surface gap and penetration correction method

The top-connection structure of a nuclear fuel assembly contains three contact surfaces, of which two are nonlinear: the contact surface between the top nozzle and the connection-sleeve outer surface and that between the connection-sleeve inner surface and the outer surface of the locking-thimble outer surface. The other is linear: the contact surface between the guide thimble and the inner surface of the connection sleeve. Therefore, for the nonlinear contact surfaces of the top-connection structure, the gap and penetration values under different mesh sizes can be established by analyzing the penetration and gap variation patterns between each contact surface under different mesh sizes, as listed in Table 2.

Table 2. Nonlinear contact surface gap and penetration values for different mesh sizes

	Connection sleeve and locking thimble contact surface					Top nozzle and connection sleeve contact surface				
	5mm	4mm	3mm	2mm	1mm	5mm	4mm	3mm	2mm	1mm
Penetration /mm	0.45	0.36	0.28	0.0006	0.0001	0.05	0.038	0.034	0.03	0.003
Gap /mm	1×10^{-5}	3×10^{-6}	2×10^{-7}	1×10^{-8}	1×10^{-9}	3×10^{-6}	2×10^{-6}	3×10^{-6}	2×10^{-7}	3×10^{-11}

As presented in Table 2, the direct penetration value of the contact surface decreases as the mesh size between each contact surface gradually decreases. The gap between each contact surface also decreases with a decrease in the mesh size.

Corrections for the gap and penetration values of the contact surfaces for different mesh sizes were performed, and the results are listed in Table 3.

Table 3. Penetration and gap correction for each contact surface with different mesh sizes

	Connection sleeve and locking thimble contact surface					Top nozzle and connection sleeve contact surface				
	5mm	4mm	3mm	2mm	1mm	5mm	4mm	3mm	2mm	1mm
Penetration/mm	0.45	0.36	0.28	0.0006	0.0001	0.05	0.038	0.034	0.03	0.003
Penetration correction /mm	2×10^{-13}	3×10^{-13}	2×10^{-13}	9×10^{-14}	3×10^{-14}	2×10^{-14}	2×10^{-13}	8×10^{-15}	5×10^{-15}	3×10^{-15}
Gap/mm	1×10^{-5}	3×10^{-6}	2×10^{-7}	1×10^{-8}	1×10^{-9}	3×10^{-6}	2×10^{-6}	3×10^{-6}	2×10^{-7}	3×10^{-11}
Gap correction /mm	0	0	0	0	0	0	0	0	0	0

As presented in Table 3, all corrected gap values were 0. It is assumed that the contact surfaces are tightly matched with no gaps. In nonlinear contact analysis, this facilitates the complete transmission of force on each contact surface, is beneficial for the convergence of the results, and ensures the accuracy of the results. The corrected penetration values for different mesh sizes were all $<10^{-13}$. Consequently, the penetration values between the contact surfaces can be considered negligible. This will assist in the adoption of a suitable mesh size to reduce the computational resources required for the assembly, as well as converge the analysis to ensure the accuracy of the results.

3. Approximation model construction method for the top-connection structure

Building a reliability approximation model is a prerequisite and foundation for reliability analysis of a system. In this study, a method and process for the construction of an assembly-oriented reliability approximation model was established using the following stages: pre-experimental design of the connection structure, sensitivity analysis of the design variables, and verification of the accuracy of the approximation model.

3.1 Pre-experimental design of top-connection structure variables

In the experimental design for assembly, unlike generic parts, the design variable

spans of parts tend to overlap. Therefore, conducting a pre-experimental design can not only verify the plausibility of multiple design variable spans of the assembly but also reduce the number of design variables and preserve those with substantial influence on the reliability response. In the mechanical analysis of the top-connection structure of the nuclear fuel assembly under transportation and lifting conditions, the loads included the weights of the fuel assembly and control-rod assembly and axial acceleration. The total weight of the payload was ~7500 N and the axial acceleration was 4 g. Based on the ASME code, the third strength theory was used to evaluate the results of this study [23]. The simulation results for the top-connection structure under the transport and lifting conditions are shown in Figure 4.

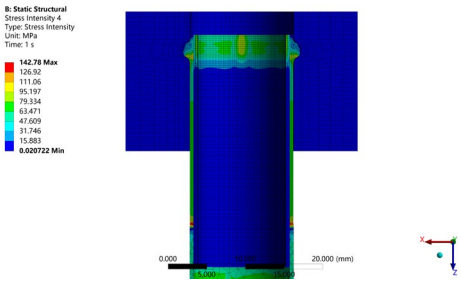

Mating surface overall stress distribution diagram

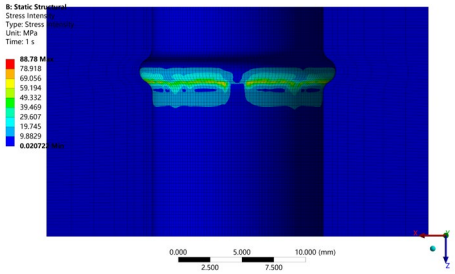

Top nozzle stress distribution diagram

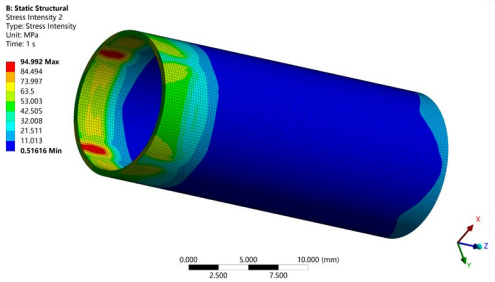

Lucking thimble stress distribution diagram

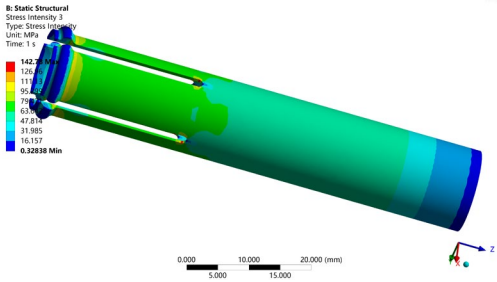

Connection sleeve stress distribution diagram

Figure 4. Stress distribution diagrams of each part

Figure 4 shows that the overall stress of the assembly under the transportation and lifting conditions is mainly distributed near the contact surface. The maximum stresses of each part are at the contact surface, being 142.78 MPa for the connection sleeve, 94.992 MPa for the locking thimble, and 88.78 MPa for the top nozzle. The maximum stress value of each part was considered as the output response, and the maximum output response of each part was parameterized to realize a closed loop between the input and output parameters. The number of top-connection structure design variables

was finally set to seven: D1, H2, R2, D5, D3, R6, and D7. The output response was set as the maximum stress value of each part from the simulation analysis, namely, Stress1, Stress2, and Stress3, corresponding to the maximum stress values of the top nozzle, locking thimble, and connection sleeve, respectively.

To ensure a uniform distribution of sample points in the design space and improve design efficiency, the Latin hypercube sampling method was deployed for the pre-experimental design of the design variables [24]. The design matrix contained 36 sample points, and the results of the pre-experimental design are presented in Appendix 1.

3.2 Sensitivity analysis of top-connection structure design variables

The number of assembly design variables is typically large, with each design variable exerting various degrees of influence on the output response. Therefore, reserving all design variables for analysis imposes a considerable burden on computational resources. Through a sensitivity analysis, the trend of the influence of each design variable on the output response, as well as the specific value of the influence, was obtained. To improve the computational efficiency, a sensitivity analysis was performed on the assembly design variables, and the design variables with a greater influence on the output response were selected to establish a reliability approximation model.

A sensitivity analysis was performed on the design variables of the top-connection structure. The extent of influence of design variables D1, H2, R2, D5, D3, R6, and D7 on the output responses Stress1, Stress2, and Stress3 are shown in Figure 5, and the specific sensitivity values of each design parameter are listed in Table 4.

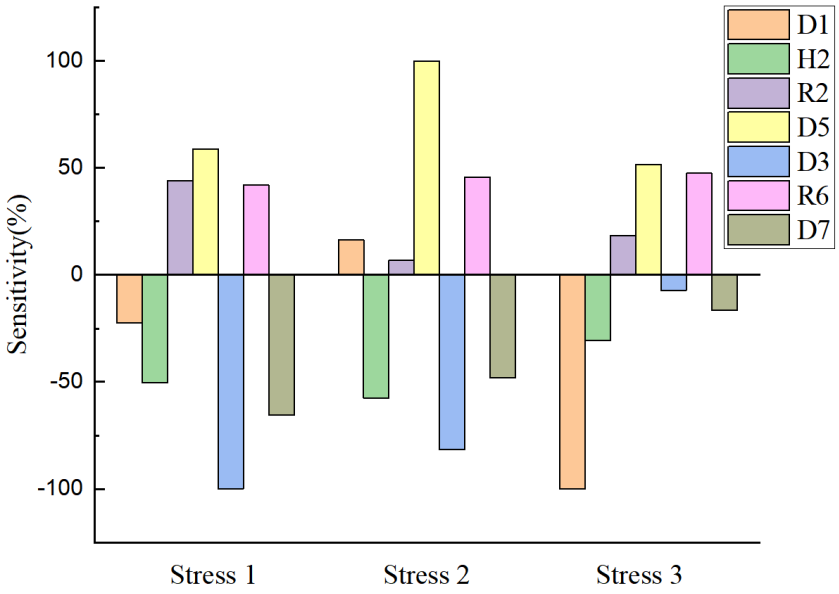

Figure 5. Extent of the influence of each parameter on the output response

Figure 5 shows that D1 demonstrated a negative correlation for both Stress1 and Stress3 and a positive correlation for Stress2. Among the design parameters, D1, D5, and D3 had the greatest influence on Stress3, Stress2, and Stress1, respectively. The extent of influence of each design parameter on Stress1 was ranked as D3 > D7 > D5 > H2 > R2 > R6 > D1, the extent of influence on Stress2 was ranked as D5 > D3 > H2 > D7 > R6 > D1 > R2, and the extent of influence on Stress3 was ranked as D1 > D5 > R6 > H2 > R2 > D7 > D3.

Table 4. Sensitivity values for each design variable

Design variable	Sensitivity		
	Stress1	Stress2	Stress3
D1	-22.50	16.35	-100
H2	-50.43	-57.53	-30.56
R2	44.04	6.82	18.25
D5	58.89	100	51.51
D3	-100	-81.57	-7.13
R6	41.95	45.71	47.45
D7	-65.62	-48.13	-16.56

The construction of the response surface of each parameter versus the output response provides a straightforward understanding of the sensitivity of each parameter to the output response. Figure 6 shows the response surface of each parameter for the output response. From the response surface of each parameter to the output, the parameters did not exhibit monotonically increasing or decreasing effects on the output

response, and a mutual influence existed between the two design variables. By taking H2 and D7 Stress1 as a reference, when D7 = 9 mm, the output response decreases monotonically with the increase in H2; when D7 = 10 mm, the output response decreases first with the increase in H2 and then increases; and, when D7 = 10.5 mm, the output response monotonically increases again with the increase in H2. When H2 = 4.5 mm, the output response increases monotonically with an increase in D7; when H2 = 5 mm, the output response decreases and then increases with an increase in D7; when H2 = 5.5 mm, the output response increases monotonically with an increase in D7.

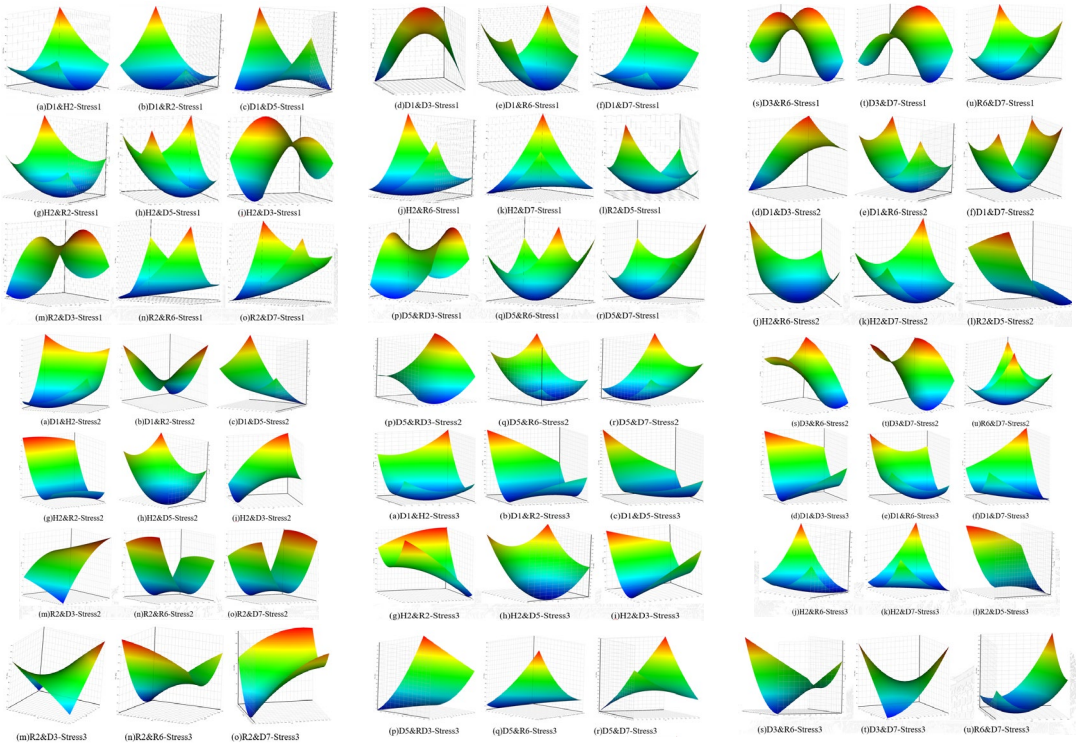

Figure 6. Response surface of each parameter to the output response

Combining the response surfaces of each design parameter for Stress1, Stress2, and Stress3 reveals that all seven design variables of the top-connection structure have a significant impact on the output response. Therefore, there is no need to scale down the design variables.

3.3 Approximation model construction for top-connection structure

The pre-experimental design and design variable sensitivity analysis identified the design variables that influence the output response. Subsequently, an experiment was conducted to identify the design variables and obtain a more accurate approximation model of reliability. Appendix 2 presents the experimental design results for the top-

connection structural variables.

The 120 generated sample points were divided into two groups, one serving as learning points to establish an approximation model and the other as verification points to assess the accuracy of the model. The principle of this division was to provide a sufficient number of learning points and reserve a certain number of verification points. Therefore, the sample points were divided in a ratio of 3:1 [25], with sample points 1–90 as the learning points and sample points 91–120 as the verification points.

The Kriging model, as an efficient interpolation method, can yield not only the predicted value of a prediction point but also the variance of that point. Because of this advantage, this method was used to construct a reliability approximation model in this study.

Assume that the actual relationship between the response and design variables can be expressed as

$$y(x) = F(x)^T \beta + z(x), \tag{1}$$

where $F(x)$ is a linear combination of polynomial functions, β is a linear regression coefficient, and $z(x)$ is a Gaussian stochastic process with a mean of 0. The covariance between the two points x_i and x_j is

$$\mathrm{Cov}[z(x_i), z(x_j)] = \sigma^2 R(x_i, x_j; \theta), \tag{2}$$

where σ is process variance, $R(x_i, x_j; \theta)$ is the correlation function at two points x_i and x_j, usually a Gaussian correlation function:

$$R(x_i, x_j; \theta) = \prod_{m=1}^{M} \exp[-\theta_m (x_i^m - x_j^m)^2], \tag{3}$$

where θ is a parameter vector, m is the mth-dimensional vector of the input vector, and M is the total dimensionality of the input vector. θ can be estimated by using the maximum likelihood method as

$$\overset{*}{\theta} = \arg\max(-N_0 \ln(\sigma^2) - \ln|R|). \tag{4}$$

A Kriging model was constructed based on n training points x_i ($i = 1, 2, \ldots, n$). Let Y represent the vector of responses at n training points. The vectors of the regression

coefficients and process variance can be estimated as

$$\overset{*}{\beta} = (F^T R^{-1} F)^{-1} F^T R^{-1} Y, \tag{5}$$

$$\sigma^2 = \frac{1}{N_0}(Y - F\overset{*}{\beta})^T R^{-1}(Y - F\overset{*}{\beta}), \tag{6}$$

$$r(x) = [R(x, x_1; \theta), R(x, x_2; \theta), ..., R(x, x_n; \theta)]^T, \mu = F(x)^T \overset{*}{\beta} + \mathrm{r}(x)^T R^{-1}(Y - F\overset{*}{\beta}). \tag{7}$$

3.4 Approximation model accuracy verification

The accuracy of the approximation model is crucial to the accuracy of the reliability analysis results, and it can be verified via validation points. The metrics for the accuracy verification of the approximation model include the relative maximum absolute error (RMAE), root mean square error (RMSE), and coefficient of determination R^2 [26,27]. RMAE is given by

$$\mathrm{RMAE} = \frac{\max\limits_{i=1:N}\{|\, y_i - \hat{y}_i \,|\}}{\sqrt{\frac{1}{N}\sum\limits_{i=1}^{N}(y_i - \overline{y}_i)^2}}, \tag{8}$$

where N is the number of verification points, y_i is the true value of the ith verification point, $\hat{y}_i$ is the predicted value of the ith verification point, and $\overline{y}$ is the mean value of the verification points. The RMAE was used to characterize the absolute maximum residual value relative to the standard deviation of the output value of the sample points. The closer the value of RMAE is to 0, the higher the accuracy of the approximation model.

RMSE is given by

$$\mathrm{RMSE} = \sqrt{\frac{1}{N}\sum_{i=1}^{N}(y_i - \hat{y}_i)^2}. \tag{9}$$

The RMSE was used to characterize the dispersion of the sample points. The closer the RMSE value is to 0, the higher the accuracy of the approximation model.

Finally, R^2 is given by

$$R^2 = 1 - \frac{\sum_{i=1}^{N}(y_i - \hat{y}_i)^2}{\sum_{i=1}^{N}(y_i - \bar{y})^2}. \tag{10}$$

R^2 was used to characterize the degree of agreement between the predicted and real values. The closer the R^2 value is to 1, the higher the accuracy of the approximation model.

Figure 7 shows the relationship between the predicted and true values, and the errors for each method are listed in Table 5.

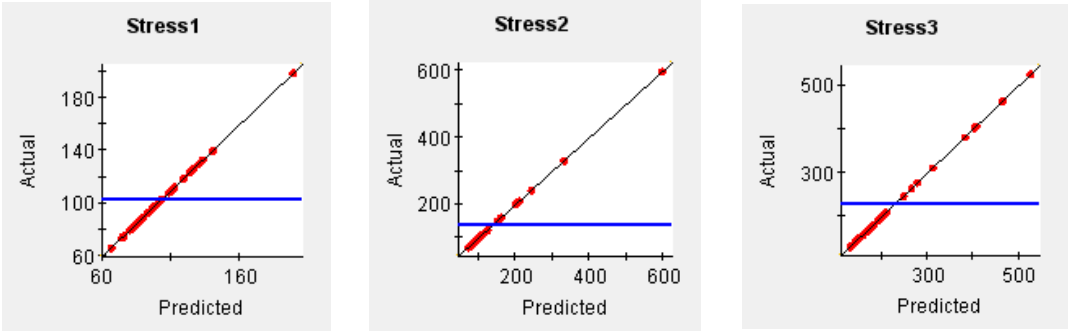

Figure 7. Kriging goodness-of-fit graphs

Table 5. Kriging model accuracy validation

	Stress1	Stress2	Stress3
RMAE	2.1×10^{-16}	1.2×10^{-15}	5.8×10^{-16}
RMSE	1.1×10^{-16}	2.7×10^{-16}	1.6×10^{-16}
R^2	1	1	1

As presented in Table 5, the results verified by each method meet the requirements and, consequently, prove that the Kriging model constructed according to this sample point meets the accuracy requirements.

4. Reliability analysis method for the top-connection structure

The top-connection structure of the nuclear fuel assembly is complex. In practical engineering, the stochasticity brought by design variables needs to be considered, as it affects the overall structure reliability. The reliability analysis flow for the top-connection structure used in this study is shown in Figure 8. The probability distribution and the type of probability distribution for each random variable in the top-connection

structure were determined. Subsequently, the limit-state function of the top-connection structure was constructed, and its reliability was calculated via MCS invoking the approximation model. This not only addressed the low calculation efficiency of the assembly system but also ensured the accuracy of the reliability analysis results.

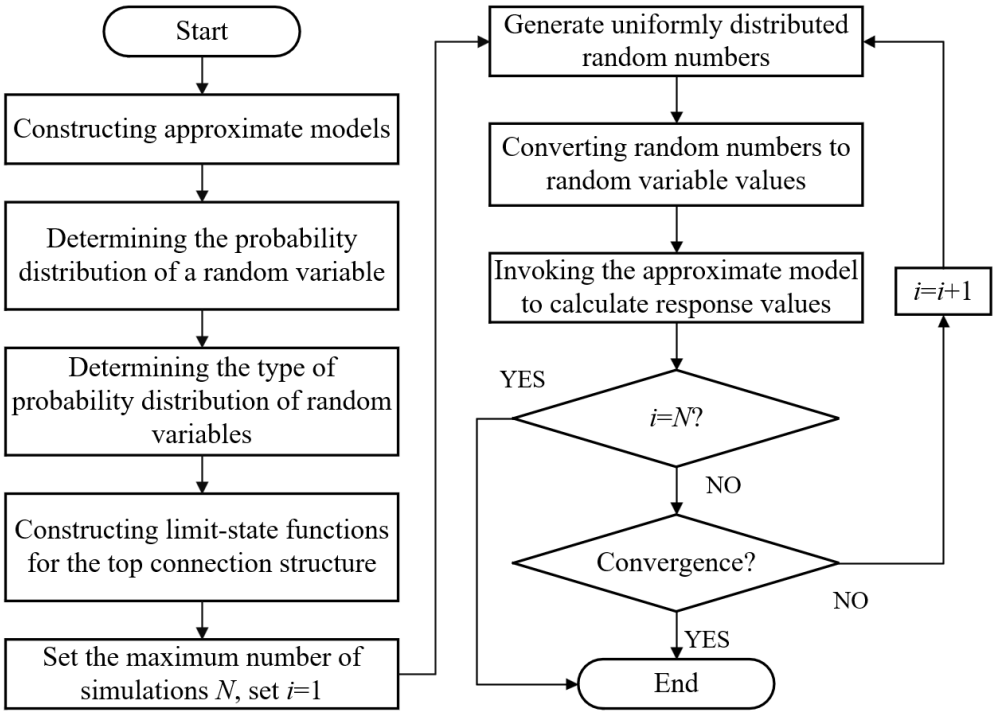

Figure 8. Assembly-oriented reliability analysis flowchart of the top-connection structure

4.1 Multivariate reliability analysis based on MCS

MCS is a robust stochastic simulation method for structural reliability analysis [28-30]. It is an excellent contemporary tool for structural reliability analysis because its calculation accuracy and convergence speed are not affected by the system complexity [31-33]. However, the computational efficiency of this method is limited and the required number of sample points is large. In light of this, to address the limited computational efficiency of MCS combining the assembly-oriented reliability approximation model, a Monte Carlo reliability analysis method based on an approximation model is proposed in this study. The specific steps are as follows:

Step 1: Determine the random variables and designate their probability distribution and probability distribution types.

Step 2: Define the maximum number of MCS simulation runs, N.

Step 3: Generate a sequence of uniformly distributed random numbers.

Step 4: Convert the generated random number sequence into corresponding random variable values.

Step 5: Invoke the assembly approximation model to compute the response to the current value.

Step 6: Repeat Steps 3–5 until the maximum number of simulations, N, is reached.

4.2 Probability distribution statistics of random variables for the top-connection structure

In machining the top-connection structure of nuclear fuel assemblies, the working accuracy varies because of the accuracy of the machine tools and instruments, as well as the proficiency of the machining operators. Therefore, reliability analysis of the top-connection structure requires considering each critical dimension as a random variable. Furthermore, the influence of material properties and the unevenness of loading on the structural function should also be considered, with the modulus of elasticity E of the material and loading force F as random variables. Under normal conditions, the dimensionality caused by machining errors conforms to a normal distribution. The part dimensions in the top-connection structure as an assembly have upper and lower limits, thus conforming to a truncated normal distribution. The modulus of elasticity E of the material follows a normal distribution, whereas the force load F fluctuates within a certain range, making it conform to a truncated normal distribution. The statistical properties of each random variable for the top-connection structure are listed in Table 6.

Table 6. Statistical properties of each random variable

Random Variable	Mean value	Lower limit value	Upper limit value	Standard deviation	Distribution Type
D1/mm	13.45	12.95	13.95	0.289	Truncated normal distribution
H2/mm	5	4.5	5.5	0.286	Truncated normal distribution
R2/mm	1	0.75	1.25	0.058	Truncated normal distribution
D5/mm	11.45	10.95	11.95	0.289	Truncated normal distribution
D3/mm	12.45	11.95	12.95	0.288	Truncated normal distribution
R6/mm	0.5	0.45	0.55	0.029	Truncated normal distribution
D7/mm	11.45	10.95	11.95	0.288	Truncated normal distribution
E/GPa	199	——	——	1.1×10^4	normal distribution
F/N	1250	1100	1400	86.243	Truncated normal distribution

4.3 Limit-state function determination for the top-connection structure

The structural output response of the top connection must satisfy the ASME code, with a membrane stress of <138 MPa and a membrane plus bending stress of <207 MPa. The failure mode of the top-connection structure is a typical strength failure, and the following structural limit-state function can be established [34]:

$$G(x_1,...,x_n) = R(x_1,...,x_n) - S(x_1,...,x_n), \tag{11}$$

where the variables $x_1,...,x_n$ are random variables affecting the function, $R(x_1,...,x_n)$ is the rigidity random variable, and $S(x_1,...,x_n)$ is the stress random variable. When $G > 0$, the structure is in a safe state, whereas, when $G < 0$, it is in a failure state.

The top-connection structure, which is an assembly composed of several parts, fails when one part fails. Therefore, they can be regarded as a system. For the top-connection structure, the specific structure limit-state function is

$$G(X) = 207 - \max\{\text{Stress}1, \text{Stress}2, \text{Stress}3\} = 0. \tag{12}$$

The probability of an individual part failure can be expressed as $P_{f_i} = P(G(x_1,\cdots,x_n) < 0)$; the probability of the entire top-connection structure failure is $P_f = P_1 \bigcap \cdots \bigcap P_i$, where i is the number of system parts and the reliability is $P_s = 1 - P_f$.

4.4 Reliability assessment method for the top-connection structure

In this study, the MCS method was deployed, invoking the Kriging model to calculate the reliability of the top-connection structure. The maximum number of runs of the MCS was set to 10,000. The distribution types and data for each random parameter are listed in Table 8. The results for each response distribution are shown in Figure 9.

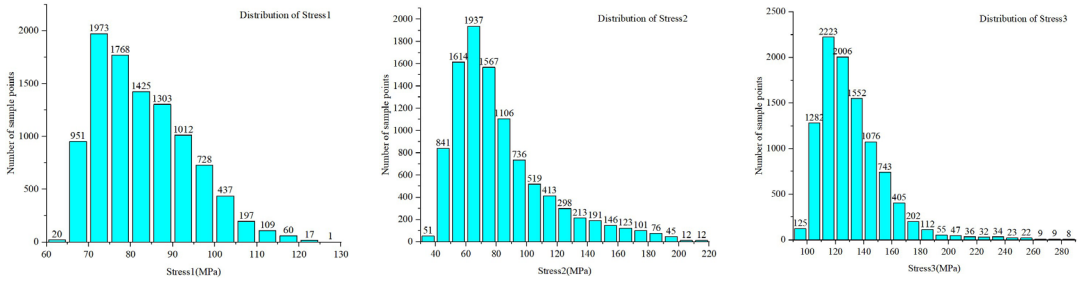

Figure 9. Cumulative distribution of each response

Figure 9 shows that the stress distributions of Stress1 are all within 130 MPa, concentrated in the range of 65–110 MPa, and do not exceed 207 MPa; the stress distributions of Stress2 are concentrated in the range of 40–110 MPa, with very few exceeding 200 MPa; and the stress distributions of Stress 3 are concentrated between 100 and 170 MPa, with a few exceeding 200 MPa. The failure probability of each part is

$$P_f = \frac{N}{N_0}, \tag{13}$$

where N is the number of sample points with $G(x) < 0$ in the MCS and N_0 is the total number of MCS runs. The failure probability of each part can be obtained from Figure 9 and is listed in Table 7.

Table 7. Probability of failure and reliability of each part

	Top nozzle	Locking thimble	Connection sleeve
Failure probability	0	0.15%	1.85%
Reliability	100%	99.85%	98.15%

According to Table 7, the reliabilities of the top nozzle, locking thimble, and connection sleeve are 100%, 99.85%, and 98.15%, respectively. This corresponds to a real-world failure scenario. The connection sleeve, placed between the top nozzle and locking thimble, was directly loaded by the entire fuel assembly during operation. Compared to the top nozzle and locking thimble, it exhibited the highest probability of failure during operation in the fuel assembly [13]. In general, the structural reliability of the top connection remained sound even when considering the randomness of each variable.

5. Conclusion

An assembly-oriented reliability analysis method for top-connection structures of nuclear fuel assemblies was presented. Based on the assembly features, a parametric modeling method for assembly systems and a design parameter correlation method were proposed, and an assembly-oriented correction method for the nonlinear contact surface gap and penetration of the top-connection structure was established to address the reliability analysis accuracy fluctuation caused by gaps and penetrations between contact surfaces during the assembly analysis. An assembly-oriented reliability analysis model for the top-connection structure was established, considering the randomization of design variables, such as machining error, material, and force load. The Kriging model and MCS method were deployed to analyze the structural reliability of the top-connection structure of the nuclear fuel assembly, and the obtained reliability of the assembly system demonstrated better agreement than the physical experimental data. The proposed method, with sound applicability and practicability, is applicable not only to the reliability analysis of the top-connection assembly structure of a nuclear fuel assembly but also for the reliability analysis of complex structures with multiple assembly relations. Notably, the material characteristics and reliability of nuclear fuel assemblies are significantly affected by the long-term operation of nuclear fuel assemblies under high temperature, high pressure, and high levels of radiation. Time-varying reliability analysis of nuclear fuel assemblies will be the focus of future studies.

Appendix 1: Pre-experimental design matrix and experiment results

Table 8. Pre-experimental design matrix and experiment results

N	D1	H2	R2	D5	D3	R6	D7	Stress1	Stress2	Stress3
1	13.263	5.347	1.058	9.688	11.750	0.540	9.896	72.371	51.022	108.638
2	13.712	5.292	0.914	9.604	11.917	0.476	10.354	63.620	42.801	102.795
3	12.142	4.875	1.008	9.021	10.917	0.493	9.396	77.481	61.728	119.617
4	13.487	5.486	0.969	9.979	10.817	0.460	9.271	93.277	124.675	137.641
5	12.292	4.847	0.964	9.396	11.783	0.549	9.313	68.693	55.227	280.260
6	14.608	4.736	0.975	9.563	11.450	0.504	9.854	76.737	74.076	124.963
7	13.413	5.014	0.997	10.479	11.017	0.471	9.021	115.021	222.975	192.132
8	14.533	4.597	1.075	10.146	11.117	0.518	9.229	101.634	144.597	153.750
9	12.665	5.181	1.053	9.313	11.083	0.538	9.938	78.716	62.022	109.951

10	12.516	5.042	1.042	10.438	11.950	0.513	9.646	87.582	78.170	250.555
11	12.890	5.236	0.992	10.188	11.550	0.501	10.021	85.274	73.190	127.772
12	12.441	4.986	1.031	10.229	10.950	0.463	10.438	104.314	164.118	180.201
13	13.188	4.625	1.069	9.438	11.217	0.482	9.688	84.632	83.386	118.151
14	13.861	4.514	0.936	9.938	11.683	0.485	9.479	96.094	84.608	125.575
15	12.815	4.569	1.036	10.104	11.717	0.507	10.271	79.923	79.896	127.995
16	14.309	5.153	0.981	9.646	11.383	0.546	9.521	74.388	67.622	115.862
17	14.160	5.264	0.908	9.271	10.983	0.529	10.146	70.514	67.236	113.680
18	13.637	5.069	1.086	9.813	10.850	0.532	10.396	95.636	120.241	143.465
19	12.367	4.708	0.953	10.063	11.317	0.474	9.979	85.478	91.709	140.391
20	12.217	4.792	1.064	9.104	11.417	0.499	10.188	68.795	55.558	174.180
21	13.114	5.208	0.919	9.188	11.583	0.490	10.229	67.741	44.310	104.815
22	14.384	5.125	0.958	10.021	11.250	0.451	10.313	90.679	96.088	133.996
23	14.683	4.764	0.986	9.146	10.883	0.496	9.563	77.036	84.775	116.305
24	12.591	5.458	1.014	9.354	11.483	0.468	9.063	71.814	52.974	129.991
25	13.936	4.542	0.942	9.771	11.050	0.524	9.438	97.981	115.708	145.906
26	13.562	4.931	1.019	10.271	11.850	0.526	10.063	70.325	72.299	117.321
27	14.085	4.903	1.047	9.896	11.883	0.521	9.104	79.176	62.089	116.681
28	13.786	5.375	1.003	9.229	11.817	0.465	9.771	74.470	38.660	101.617
29	14.758	4.681	1.097	9.479	11.650	0.457	10.479	71.423	66.579	120.725
30	12.964	5.319	0.947	10.396	11.150	0.535	10.104	97.230	136.076	143.181
31	14.010	4.958	0.925	9.729	11.983	0.488	9.188	67.129	52.081	100.040
32	14.235	5.403	1.092	10.354	11.283	0.515	9.354	85.644	113.930	144.575
33	13.338	4.819	0.931	9.521	11.183	0.543	9.729	76.460	79.474	119.466
34	14.459	5.431	1.025	9.854	11.517	0.510	9.813	78.493	62.743	111.810
35	13.039	5.097	1.081	9.063	11.617	0.454	9.146	70.461	44.578	98.405
36	12.740	4.653	0.903	10.313	11.350	0.479	9.604	118.836	123.310	153.071

Appendix 2: Experimental design matrix and experimental results

Table 9. Experimental design matrix and experimental results

N	Design variables									Results		
	D1	H2	R2	D3	R6	D5	D7	E	F	Stress1	Stress2	Stress3
1	13.25	4.86	0.92	12.95	0.46	11.61	11.83	1.93×10^5	1101.25	65.68	81.42	389.75
2	13.50	5.18	1.07	12.68	0.55	11.10	11.59	2.01×10^5	1228.75	73.93	71.44	168.58
3	12.96	5.25	0.91	12.19	0.47	11.02	11.91	1.91×10^5	1206.25	95.50	85.70	181.00
4	13.38	4.74	1.01	12.88	0.47	11.11	10.99	2.09×10^5	1218.75	71.26	67.24	266.04
5	13.00	4.62	1.07	12.13	0.45	11.27	11.09	2.16×10^5	1161.25	94.16	132.11	160.55
6	13.87	4.99	1.09	12.18	0.51	11.41	11.65	2.08×10^5	1178.75	96.32	144.17	160.76
7	13.32	5.07	0.92	12.12	0.47	11.82	11.55	1.98×10^5	1118.75	154.56	338.55	220.15
8	13.86	4.77	0.99	12.55	0.52	11.90	11.94	1.91×10^5	1168.75	117.22	172.13	183.66
9	13.09	4.51	0.99	12.23	0.45	11.75	11.20	2.14×10^5	1361.25	167.36	298.76	222.34
10	13.03	4.94	1.02	12.83	0.48	11.36	11.28	2.17×10^5	1123.75	85.13	85.60	592.49
11	13.18	4.75	0.90	12.70	0.52	11.85	11.53	1.97×10^5	1286.25	99.03	116.96	307.71
12	13.02	4.57	1.00	12.10	0.53	11.16	11.90	1.93×10^5	1143.75	93.22	118.55	148.49
13	13.21	5.00	0.94	12.73	0.51	10.97	11.26	1.92×10^5	1273.75	70.36	69.97	290.51
14	13.55	5.33	0.96	12.03	0.50	11.15	11.14	2.02×10^5	1343.75	106.86	109.52	161.00
15	13.14	5.01	0.96	12.05	0.49	11.01	11.80	1.84×10^5	1311.25	83.56	95.32	145.15
16	13.70	4.65	0.95	12.61	0.49	11.21	11.76	2.15×10^5	1211.25	101.60	79.63	131.04
17	13.67	4.97	1.03	12.24	0.49	11.85	11.66	1.94×10^5	1303.75	171.80	304.14	244.58
18	13.46	5.11	1.09	12.85	0.51	11.33	11.74	1.92×10^5	1231.25	74.89	76.50	219.69
19	13.00	4.78	0.97	12.30	0.50	11.03	11.51	2.07×10^5	1398.75	104.65	96.00	229.98

20	12.99	5.24	1.05	12.26	0.51	11.20	10.96	1.94×10^5	1166.25	90.69	90.54	187.89
21	13.20	4.75	1.06	12.92	0.50	11.44	11.81	2.01×10^5	1263.75	67.36	88.74	485.62
22	13.71	4.88	0.95	12.05	0.47	11.47	11.25	1.87×10^5	1146.25	107.22	189.21	171.78
23	13.90	4.72	0.98	12.65	0.54	11.30	11.40	1.99×10^5	1253.75	91.27	81.88	144.70
24	13.05	5.29	1.01	12.40	0.49	11.40	11.24	1.89×10^5	1328.75	95.85	101.76	240.73
25	13.58	5.47	1.07	12.32	0.46	11.80	11.30	1.80×10^5	1236.25	123.60	148.44	165.35
26	13.45	5.48	1.05	11.95	0.53	11.12	11.27	1.85×10^5	1183.75	103.32	96.60	135.32
27	13.65	4.82	1.04	11.96	0.53	11.60	11.20	2.02×10^5	1148.75	165.33	332.65	215.14
28	13.45	5.00	1.00	12.45	0.50	11.45	11.45	1.99×10^5	1250	88.78	94.99	142.78
29	13.91	5.45	0.95	12.27	0.55	11.35	11.38	2.06×10^5	1196.25	90.99	86.63	142.73
30	13.19	5.03	1.08	11.98	0.48	11.26	11.37	1.96×10^5	1181.25	102.47	141.68	157.56
31	13.61	4.58	1.04	12.60	0.52	11.76	11.62	2.14×10^5	1116.25	102.12	135.00	144.08
32	13.68	4.76	1.06	12.89	0.52	11.46	11.58	1.99×10^5	1251.25	86.72	75.89	176.46
33	13.29	5.02	0.97	12.85	0.50	11.93	11.79	2.13×10^5	1318.75	92.66	115.60	331.62
34	13.72	5.45	1.10	12.53	0.51	11.31	11.75	1.93×10^5	1238.75	78.62	78.10	122.03
35	13.20	5.12	0.97	12.34	0.48	11.45	11.71	1.88×10^5	1348.75	107.30	110.30	183.24
36	13.10	4.55	1.08	12.59	0.51	11.23	11.36	1.96×10^5	1386.25	94.41	96.77	304.19
37	13.80	4.96	1.08	12.87	0.49	11.50	11.03	1.97×10^5	1111.25	80.50	66.96	131.18
38	13.79	5.10	0.93	12.07	0.53	11.30	11.46	2.04×10^5	1158.75	106.18	129.99	146.99
39	13.42	5.13	0.93	12.20	0.52	11.70	11.75	2.12×10^5	1291.25	132.42	185.09	330.75
40	13.92	5.17	0.91	12.75	0.49	11.88	11.04	1.80×10^5	1326.25	124.43	100.78	161.07
41	13.40	4.80	0.91	12.90	0.50	11.49	11.67	1.86×10^5	1113.75	67.76	71.96	239.71
42	13.30	4.59	0.90	12.40	0.49	11.08	11.25	1.83×10^5	1186.25	91.21	80.74	152.56
43	13.56	4.85	0.95	12.02	0.49	11.92	11.05	2.10×10^5	1388.75	320.24	2051.87	519.45
44	13.06	5.19	1.02	12.86	0.55	11.57	11.05	2.19×10^5	1366.25	82.46	110.24	736.30
45	13.64	5.37	0.92	12.84	0.47	10.99	11.44	2.08×10^5	1346.25	83.03	63.23	185.71
46	13.57	4.90	0.96	12.36	0.53	11.89	11.12	1.87×10^5	1391.25	139.38	258.13	208.50
47	13.76	4.66	0.94	12.94	0.46	11.06	11.23	1.98×10^5	1256.25	71.93	60.22	165.41
48	13.53	5.35	1.04	12.56	0.45	10.95	11.13	2.03×10^5	1133.75	67.20	61.57	131.49
49	13.12	4.67	0.95	12.17	0.52	11.22	11.40	1.99×10^5	1241.25	99.09	114.70	154.85
50	12.95	5.22	0.96	12.50	0.54	11.42	11.89	1.85×10^5	1298.75	97.49	101.00	328.55
51	13.05	5.34	1.08	11.99	0.50	11.94	11.56	1.95×10^5	1358.75	568.32	4072.76	847.39
52	13.62	5.50	1.06	12.72	0.52	11.71	11.10	1.86×10^5	1353.75	102.55	95.37	170.87
53	13.78	5.32	0.92	12.45	0.54	11.19	11.92	2.10×10^5	1203.75	89.50	68.21	127.77
54	13.59	4.79	1.04	12.65	0.46	11.55	11.45	1.81×10^5	1243.75	96.02	90.52	150.04
55	13.25	5.49	1.10	12.70	0.52	11.52	11.10	2.08×10^5	1176.25	79.44	90.46	247.28
56	13.35	4.95	0.99	12.69	0.51	11.86	11.54	2.18×10^5	1306.25	100.49	120.63	227.94
57	13.69	4.91	0.91	12.47	0.46	11.24	11.69	2.06×10^5	1128.75	94.18	72.17	130.80
58	13.60	5.27	0.91	12.25	0.49	11.43	11.55	2.06×10^5	1296.25	108.21	103.68	151.50
59	13.34	5.40	1.02	12.51	0.48	11.00	11.64	1.86×10^5	1156.25	72.74	68.06	159.67
60	13.90	4.81	1.00	12.64	0.51	11.32	11.57	2.12×10^5	1221.25	94.29	77.33	134.94
61	12.97	5.35	1.09	12.54	0.47	11.38	11.41	2.18×10^5	1316.25	93.39	106.13	349.30
62	13.47	4.55	0.93	12.15	0.55	11.69	11.02	2.03×10^5	1233.75	127.59	285.42	197.43
63	13.44	4.87	1.03	12.66	0.52	11.04	11.88	1.91×10^5	1363.75	84.98	75.21	197.95
64	13.85	4.61	1.07	12.38	0.53	11.13	11.49	1.96×10^5	1271.25	96.33	107.39	144.77
65	13.22	5.39	0.99	12.37	0.46	11.14	11.22	2.04×10^5	1283.75	94.85	86.82	174.50
66	13.80	5.04	1.01	12.22	0.47	11.66	11.52	2.03×10^5	1258.75	122.59	197.27	189.58
67	13.50	4.83	1.03	12.58	0.50	11.65	11.65	1.89×10^5	1331.25	106.61	114.17	163.73
68	13.88	5.41	1.09	12.52	0.46	11.15	11.93	2.13×10^5	1266.25	81.42	69.63	136.90
69	13.40	5.38	1.05	12.50	0.53	11.45	11.86	2.09×10^5	1191.25	94.42	87.70	152.84
70	13.89	5.25	1.10	12.00	0.51	11.05	11.95	2.05×10^5	1163.75	87.05	98.35	128.72
71	13.60	4.92	1.07	12.16	0.48	11.67	11.90	1.83×10^5	1308.75	142.32	236.27	205.51
72	13.17	4.70	0.96	12.55	0.53	11.29	11.45	2.10×10^5	1226.25	79.47	87.73	223.83
73	13.84	5.08	0.97	12.39	0.47	11.73	11.87	1.79×10^5	1383.75	129.91	174.38	181.78

74	13.13	4.80	1.04	12.31	0.54	11.83	11.60	1.88×10^5	1356.25	144.24	243.30	199.83
75	13.51	5.14	0.91	12.00	0.52	11.56	11.61	1.98×10^5	1333.75	148.03	260.73	204.39
76	13.41	5.44	1.09	12.35	0.49	11.91	11.31	2.04×10^5	1301.25	157.11	201.56	194.92
77	13.36	5.00	0.94	12.62	0.48	11.84	11.42	2.01×10^5	1193.75	104.63	112.33	184.03
78	13.16	5.46	0.99	12.11	0.54	11.87	11.73	2.17×10^5	1131.25	158.52	381.15	240.04
79	13.39	4.69	1.06	12.48	0.48	11.10	11.18	1.95×10^5	1396.25	95.26	87.58	175.54
80	13.73	5.09	1.01	12.91	0.48	11.59	10.95	2.07×10^5	1208.75	80.28	76.26	164.02
81	13.82	4.73	1.03	12.20	0.51	11.62	11.34	2.11×10^5	1151.25	117.85	200.77	183.19
82	13.74	4.56	1.02	12.57	0.53	10.98	11.39	1.84×10^5	1201.25	73.08	73.65	114.96
83	13.43	4.90	1.06	12.33	0.51	11.60	11.15	1.81×10^5	1381.25	127.03	154.60	173.81
84	13.70	4.68	1.04	12.71	0.54	11.09	11.11	1.97×10^5	1373.75	92.43	65.72	245.16
85	13.75	5.16	0.93	12.15	0.54	11.20	11.06	1.99×10^5	1171.25	85.65	95.75	144.25
86	13.07	5.30	1.01	12.81	0.51	11.63	11.77	2.17×10^5	1276.25	83.49	106.68	547.89
87	13.54	5.23	0.92	12.42	0.50	11.05	11.15	2.16×10^5	1368.75	90.69	78.46	139.47
88	13.31	4.64	1.05	12.30	0.45	11.65	11.60	2.15×10^5	1293.75	149.23	204.59	184.65
89	13.01	4.84	1.09	12.10	0.50	11.72	11.43	1.90×10^5	1138.75	139.41	296.50	197.25
90	13.85	5.28	0.93	11.97	0.48	11.54	11.21	1.90×10^5	1223.75	132.20	234.56	185.81
91	13.30	4.70	1.01	12.08	0.46	11.70	11.30	2.18×10^5	1153.75	139.96	331.49	198.89
92	13.83	5.31	0.95	12.06	0.47	11.37	11.16	2.11×10^5	1393.75	125.98	160.64	174.47
93	13.15	5.20	0.98	12.29	0.50	11.48	11.29	1.95×10^5	1213.75	108.25	108.96	164.78
94	13.27	5.05	0.96	12.90	0.54	11.79	11.47	2.15×10^5	1278.75	100.90	76.56	381.15
95	13.26	4.54	1.06	12.41	0.46	11.00	11.08	2.00×10^5	1248.75	86.92	81.70	168.28
96	13.66	4.71	0.93	12.25	0.52	11.75	10.97	2.14×10^5	1313.75	132.79	243.02	202.39
97	13.11	5.06	1.00	12.75	0.54	11.18	11.70	1.83×10^5	1336.25	88.85	83.07	402.50
98	13.48	5.43	1.03	12.79	0.48	11.25	11.00	2.05×10^5	1288.75	81.35	77.71	209.15
99	13.63	4.60	1.08	12.14	0.53	11.50	11.00	1.94×10^5	1198.75	129.75	209.66	181.12
100	13.49	4.65	0.98	12.46	0.54	10.96	11.19	1.89×10^5	1173.75	74.67	71.44	130.57
101	13.81	4.89	0.94	12.63	0.46	11.74	11.78	2.05×10^5	1341.25	103.31	123.52	159.00
102	13.35	4.98	0.98	12.44	0.46	11.90	11.85	1.82×10^5	1106.25	110.38	157.44	167.59
103	13.08	4.50	1.02	12.04	0.50	11.78	11.70	2.09×10^5	1246.25	198.78	597.87	278.00
104	13.94	4.60	1.05	12.60	0.53	11.34	11.72	2.11×10^5	1376.25	112.22	111.02	152.34
105	13.10	5.05	0.94	12.43	0.55	11.55	10.98	1.84×10^5	1121.25	83.44	97.77	196.20
106	13.52	5.21	0.97	12.01	0.48	11.35	11.35	1.88×10^5	1268.75	118.82	149.98	173.65
107	13.93	5.20	1.03	12.35	0.45	11.53	11.32	2.13×10^5	1141.25	92.89	111.00	149.01
108	12.98	5.42	0.98	12.74	0.54	11.95	11.07	2.00×10^5	1136.25	125.69	119.00	525.13
109	13.24	4.95	0.90	12.28	0.45	11.25	11.80	2.12×10^5	1188.75	85.14	89.75	144.63
110	13.15	4.93	1.07	12.67	0.47	11.68	11.85	2.02×10^5	1338.75	100.57	111.93	311.31
111	13.04	5.40	1.00	12.77	0.49	11.40	11.17	1.81×10^5	1108.75	66.20	83.20	463.98
112	13.33	4.85	0.97	12.82	0.53	11.58	11.35	1.85×10^5	1126.25	74.18	82.46	246.91
113	13.28	5.10	0.94	12.93	0.47	11.64	11.33	1.82×10^5	1323.75	75.48	93.48	406.77
114	13.37	5.26	0.92	12.80	0.48	11.07	11.63	2.07×10^5	1378.75	89.43	71.28	264.36
115	13.95	5.15	1.02	12.76	0.46	11.77	11.48	1.80×10^5	1261.25	97.73	89.91	140.54
116	13.77	5.15	0.99	12.78	0.50	11.81	11.01	1.87×10^5	1351.25	95.78	99.06	152.18
117	13.23	5.30	1.00	12.45	0.54	11.28	11.68	1.90×10^5	1281.25	79.78	89.59	191.14
118	13.75	5.36	0.98	12.49	0.55	11.39	11.82	2.16×10^5	1216.25	85.45	77.25	134.50
119	13.45	4.63	1.08	12.21	0.52	11.51	11.50	2.00×10^5	1321.25	123.43	200.83	182.56
120	13.65	4.53	1.05	12.80	0.49	11.80	11.50	1.92×10^5	1103.75	92.87	104.34	146.86

Declaration of competing interest

The authors declare that they have no competing financial interests or personal

relationships that may have influenced the work reported in this study.

Acknowledgments

This work was supported by the National Natural Science Foundation of China (No. 52075350), the Major Science and Technology Projects of Sichuan Province (2022ZDZX0001), and the Special City School Strategic Cooperation Project of Sichuan University and Zigong (No. 2021CDZG-3).

References

1. E.B. Agyekum, M.N.S. Ansah, K.B. Afornu. Nuclear energy for sustainable development: SWOT analysis on Ghana's nuclear agenda. Energy Rep. 6: 107-115(2020). https://doi.org/10.1016/j.egyr.2019.11.163
2. X.P. Guo, X.D. Guo. Nuclear power development in China after the restart of new nuclear construction and approval: A system dynamics analysis. Renew. Sust. Energ. Rev. 57: 999-1007(2016). https://doi.org/10.1016/j.rser.2015.12.190
3. S.T. Ling, W.Q. Li, C.X. Li et al. Flow field fusion simulation method based on model features and its application in CRDM. Nucl. Sci. Tech. 33(3): 1-14(2022). https://doi.org/10.1007/s41365-022-01022-0
4. D. Fan, T. Peng, Y Tang et al. Periodicity and transversal pressure distribution in a Wire‐wrapped 19‐Pin fuel assembly. Int. J. Energy Res. 45(8): 11837-11850(2020). https://doi.org/10.1002/er.5809
5. V.I. Skalozubov, I.L. Kozlov, Y.A. Komarov et al. Analysis of nuclear safety in diversification of Westinghouse fuel assemblies at WWER-1000. Ядерна фізика та енергетика. 20(2): 159-163(2019).
6. X. Wang, D. Wang, Q. Deng et al. Simulation of dynamic characteristics of NHR200-II fuel assembly. Nucl. Eng. Des. 379: 111255(2020). https://doi.org/10.1016/j.nucengdes.2021.111255
7. NB/T 20057.3-2012. Reactor system design for pressurized water reactor nuclear power plants-core part 3: fuel assemblies(2012).

8. G. Yadigaroglu, M. Andreani, J. Dreier et al. Trends and needs in experimentation and numerical simulation for LWR safety. Nucl. Nucl. Eng. Des. 221(1-3): 205-223(2003). https://doi.org/10.1016/S0029-5493(02)00339-4
9. D. Mourtzis. Simulation in the design and operation of manufacturing systems: state of the art and new trends. Int. J. Prod. Res. 58(7): 1927-1949(2020). https://doi.org/10.1080/00207543.2019.1636321
10. M. Wang, Y. Wang, W. Tian et al. Recent progress of CFD applications in PWR thermal hydraulics study and future directions. Ann. Nucl. Energy. 150, 107836 (2021).http://doi.org:10.1016/j.anucene.2020.107836.
11. Y. Wang, M. Wang, H. Ju et al. CFD simulation of flow and heat transfer characteristics in a 5× 5 fuel rod bundles with spacer grids of advanced PWR. Nucl. Eng. Technol. 52(7): 1386-1395(2020). https://doi.org/10.1016/j.net.2019.12.012
12. J. Zhang, M. Wang, C. Chen et al. CFD investigation of the cold wall effect on CHF in a 5×5 rod bundle for PWRs. Nucl. Eng. Des. 387: 111589(2022). https://doi.org/10.1016/j.nucengdes.2021.111589
13. H. Wang, Z. Pu, F. Zhu et al. Simulation and Analysis of New-Type Fuel Assembly Top Connection Structure. Nucl. Power Eng. 38(06):163-166(2017). doi: 10.13832/j.jnpe.2017.06.0163
14. S. Liu. Strength Analysis of Pipe Seat Transport and Hoisting Conditions on PWR Fuel Assembly. Southwest Petroleum University, 2019.
15. Y. Yoo, K. Kim, K. Eom et al. Finite element analysis of the mechanical behavior of a nuclear fuel assembly spacer grid. Nucl. Eng. Des. 352: 110179(2019). https://doi.org/10.1016/j.nucengdes.2019.110179
16. M.H. Duan, M.F. Zhao. A Numerical Research of the Resistance Characteristics of the Bottom Nozzle in the Annular Fuel Assembly. International Conference on Nuclear Engineering. American Society of Mechanical Engineers. 51494: V06BT08A046(2018). https://doi.org/10.1115/ICONE26-82259
17. C.Y. Wu, M.T. Kao, C.C. Chieng et al. CFD Analysis of PWR Core Top Region: Top Fuel Assembly and Top Nozzle Regions. International Conference on Nuclear Engineering. 49309: 557-564(2010). https://doi.org/10.1115/ICONE18-29463

18. M. Su, P. Chen, L. Kuang et al. Mechanical property Study of CF3 fuel assembly Bottom Nozzle. Nucl. Power Eng. 39(S1): 62-65(2018). doi: 10.13832/j.jnpe.2018.S1.0062
19. Z. Wei, S. Du, X. Wang et al. Numerical Simulation Study on Resistance Characteristics of Top Nozzle in Fuel Assembly Based on CFD. Nucl. Power Eng. 38(S2):29-33(2017). doi: 10.13832/j.jnpe.2017.S2.0029
20. Š Dyk, V. Zeman. Impact vibrations of guide thimbles in nuclear fuel assembly. Aech. Appl. Mech. 87(2): 231-244(2017). https://doi.org/10.1007/s00419-016-1189-6
21. Y. Xu, M. Conner, K. Yuan et al. Study of impact of the AP1000® reactor vessel upper internals design on fuel performance. Nucl. Eng. Des. 252: 128-134(2012). https://doi.org/10.1016/j.nucengdes.2012.06.036
22. J. Zhao, S. Xu, W. Pan et al. A Detailed Model to Predict Mechanical Characteristics of Fuel Assembly. International Conference on Nuclear Engineering. American Society of Mechanical Engineers 86366: V002T02A043(2022). https://doi.org/10.1115/ICONE29-91931
23. ASME. Section III Division 1-Subsection NG, Core support structures, 2003.
24. D. Meng, Y. Li, C. He et al. Multidisciplinary design for structural integrity using a collaborative optimization method based on adaptive approximation modelling. Mater. Des. 206: 109789(2021). https://doi.org/10.1016/j.matdes.2021.109789
25. S. Ling, W. Li, T. Yu et al. Analysis and optimization research on latch life of control rod drive mechanism based on approximate model. Nucl. Eng. Technol. 53(12): 4166-4178(2021). https://doi.org/10.1016/j.net.2021.06.012
26. R. Jin, W. Chen, T.W. Simpson. Comparative studies of metamodelling techniques under multiple modelling criteria. Struct. Multidiscip. O. 23(1): 1-13(2001). https://doi.org/10.1007/s00158-001-0160-4
27. T. Chai, R. R. Draxle. Root mean square error (RMSE) or mean absolute error (MAE)?–Arguments against avoiding RMSE in the literature. Geosci. Model Dev. 7(3): 1247-1250(2014). https://doi.org/10.5194/gmd-7-1247-2014
28. R. Y. Rubinstein, B. Melamed. Modern simulation and modeling. New York: Wiley,

1998.

29. Q. Pan, D. Dias. An efficient reliability method combining adaptive support vector machine and Monte Carlo simulation. Struct. Safety. 67: 85-95(2017). https://doi.org/10.1016/j.strusafe.2017.04.006
30. Z. Wang, M. Broccardo, J. Song. Hamiltonian Monte Carlo methods for subset simulation in reliability analysis. Struct. Safety. 76: 51-67(2019). https://doi.org/10.1016/j.strusafe.2018.05.005
31. D.V. Dao, H. Adeli, H.B. Ly et al. A sensitivity and robustness analysis of GPR and ANN for high-performance concrete compressive strength prediction using a Monte Carlo simulation. Sustainability. 12(3): 830(2020). https://doi.org/10.3390/su12030830
32. B.T. Pham, M.D. Nguyen, D.V. Dao et al. Development of artificial intelligence models for the prediction of Compression Coefficient of soil: An application of Monte Carlo sensitivity analysis. Sci. Total Environ. 679: 172-184(2019). https://doi.org/10.1016/j.scitotenv.2019.05.061
33. S. Mordechai. Applications of Monte Carlo method in science and engineering. InTech, 2011.
34. S.A. Olatubosun, Z. Zhang. Dependency consideration of passive system reliability by coupled stress-strength interference/functional relations of parameters approach. Reliab. Eng. Syst. Safe. 188: 549-560(2019). https://doi.org/10.1016/j.ress.2019.04.009